Transport and diffusion of overdamped Brownian particles in random potentials

Marc Suñé Simon,[1,*] J. M. Sancho,[1,†] and Katja Lindenberg[2,‡]

[1]*Departament d'Estructura i Constituents de la Matèria, Facultat de Física, Universitat de Barcelona, Diagonal 647, E-08028 Barcelona, Spain*

[2]*Department of Chemistry and Biochemistry and BioCircuits Institute, University of California San Diego, 9500 Gilman Drive, La Jolla, California 92093-0340, USA*

(Received 30 August 2013; published 2 December 2013)

We present a numerical study of the anomalies in transport and diffusion of overdamped Brownian particles in totally disordered potential landscapes in one and in two dimensions. We characterize and analyze the effects of three different disordered potentials. The anomalous regimes are characterized by the time exponents that exhibit the statistical moments of the ensemble of particle trajectories. The anomaly in the transport is always of the subtransport type, but diffusion presents a greater variety of anomalies: Both subdiffusion and superdiffusion are possible. In two dimensions we present a mixed anomaly: subdiffusion in the direction perpendicular to the force and superdiffusion in the parallel direction.

DOI: 10.1103/PhysRevE.88.062105 PACS number(s): 05.40.−a, 02.50.Ey, 05.60.−k

I. INTRODUCTION

Brownian particles moving in a potential landscape and perhaps also driven by an external force have been a subject of study for many decades. The label Brownian indicates particles that, in addition to a variety of possible potential landscapes and driving forces, are subject to thermal random forces and the concomitant friction embodied in the fluctuation-dissipation relation.

The interest in Brownian motion in random potentials goes back a few decades. The main focus at that time was on the effects of such potentials on diffusion [1–3] and, more recently, on the mobility [4] or on both [5]. All of these studies assumed normal behavior of both quantities. A recent upsurge of interest in these systems has come about because of the observation of a variety of qualitative anomalies such as nondiffusive regimes [6] and other "abnormal" behaviors (see references in Ref. [7]).

In this anomalous scenario, either in the absence [8] or, more recently, in the presence of an external force [7,9], numerical [7–13] and experimental [14,15] works have focused on the effects of a random contribution to the potential on Brownian motion. Indeed, the anomalies in both transport and diffusion caused by even a small amount of disorder can be very pronounced [12].

Many realistic physical systems are well described by Brownian motion in disordered media. Examples include DNA dynamics [1,16] and propagation of macromolecules and organelles in the cytoplasm of a cell. Such disordered systems are often described as crowded environments (dynamical disorder) [17]. This type of disorder is beyond the scope of this paper. Our focus in this paper is on the description of the motion of overdamped Brownian particles in a totally disordered static potential and subject to a constant external force. This scenario might describe the transport of particles in disordered solids [18–21]. By totally disordered potentials we mean that there is no systematic part in the potential other than the constant force. We rely on stochastic simulations of overdamped Brownian particles to observe and characterize those regimes that are anomalous: subtransport, subdiffusion, and superdiffusion.

The outline of this paper is as follows. In Sec. II we present a number of definitions, the dynamical equations, and a detailed characterization of disorder. In Sec. III we present numerical simulation results for a 1D spatial landscape and characterize the different anomalous regimes. In Sec. IV we discuss the evolution of the particle density in the different regimes. In Sec. V we address the problem in a 2D space. We separate the discussion in the directions parallel and perpendicular to the applied force and consider the anomalies appearing in each of these directions. Finally, in Sec. VI we conclude with some comments and conclusions.

II. DISORDERED SCENARIO

We consider the motion of overdamped independent Brownian particles evolving in a potential V and subject to a constant external force F. In one dimension the trajectory of a particle evolves according to the Langevin equation

$$\gamma \frac{dx}{dt} = -\frac{dV(x)}{dx} + F + \xi(t), \tag{1}$$

where x is the position of the particle, t is the time, γ is the friction parameter, F is the applied external force, $V(x)$ is a disordered potential, and $\xi(t)$ is the thermal noise at temperature T, which is a Gaussian stochastic process with zero mean and a correlation function that obeys the fluctuation-dissipation relation $\langle \xi(t)\xi(t')\rangle = 2k_B T\gamma\delta(t-t')$. Here k_B is the Boltzmann constant and the angular brackets denote statistical averages. The totally disordered potential $V(x)$ is characterized by its statistical properties, in particular by its mean $\langle V(x)\rangle$, which we take to be zero, and its correlation function $\langle V(x)V(x')\rangle$, where the angular brackets now indicate a spatial average. We assume that this correlation function has a characteristic length λ_r.

To minimize the number of independent parameters, we introduce a length scale λ_0, an energy scale V_0, and a time scale t_0 related to the first two as $t_0 = \gamma\lambda_0^2/V_0$. That leaves

*sune@ecm.ub.edu
†jmsancho@ecm.ub.edu
‡klindenberg@ucsd.edu

us with just three parameters λ_0, V_0, and γ in addition to the temperature. We furthermore introduce dimensionless variables z and τ,

$$z = \frac{x}{\lambda_0}, \quad \tau = \frac{t}{t_0}, \tag{2}$$

and scaled dimensionless quantities

$$\hat{V}(x) = \frac{V(x)}{V_0}, \quad \mathcal{F} = \frac{\lambda_0}{V_0}F, \quad \mathcal{T} = \frac{k_B T}{V_0} \tag{3}$$

to write the equation of motion in dimensionless form

$$\frac{dz}{d\tau} = -\frac{d\hat{V}(z/\lambda)}{dz} + \mathcal{F} + \hat{\xi}(\tau), \tag{4}$$

where the fluctuation-dissipation relation now reads $\langle\hat{\xi}(\tau)\hat{\xi}(\tau')\rangle = 2\mathcal{T}\delta(\tau - \tau')$.

The totally disordered potential $\hat{V}(z/\lambda)$ has a dimensionless length scale $\lambda = \lambda_r/\lambda_0$, where λ_r is its characteristic length introduced earlier. The potential is characterized by the parameter λ and by the statistical properties. We will assume that $\hat{V}$ is a Gaussian variable, with zero mean and correlation function $g(|z|/\lambda)$,

$$\langle\hat{V}(z/\lambda)\,\hat{V}(z'/\lambda)\rangle = g(|z - z'|/\lambda). \tag{5}$$

It has recently been established [12] that the parameters λ, $\mathcal{F}$, and $\mathcal{T}$ influence the transport and diffusion anomalies in various pronounced ways. Our first goal in this work is to explore whether the functional form of the correlation function $g(|z|/\lambda)$ also affects transport and diffusion phenomena. To explore this point we consider three very different types of disordered potentials: (i) the well known normal or Gaussian form

$$g(|z - z'|) = \tfrac{1}{2}e^{-[(z-z')^2/2\lambda^2]}, \tag{6}$$

which is used here as the reference scenario because it has a well defined characteristic short spatial length scale λ and no singularity in the entire domain; (ii) the double-sided exponential correlation

$$g(|z - z'|) = \tfrac{1}{2}e^{-[|z-z'|/\lambda]}, \tag{7}$$

whose underlying force $-d\hat{V}_r/dz$ exhibits a singularity at the origin in the form of a delta correlation $\delta(z - z')$, much like spatial white noise; and (iii) a correlation function with a power-law tail

$$g(|z - z'|) = \frac{1}{2}\left(1 + \frac{(z - z')^2}{\lambda^2}\right)^{-\varepsilon/2}. \tag{8}$$

The decay of the tail is determined by the exponent ε and by a short spatial length scale λ.

From these correlations, the statistical properties of the corresponding random forces $\mathcal{F}_r$ can be obtained

$$\langle\mathcal{F}_r(z)\mathcal{F}_r(z')\rangle = -\frac{\partial^2 g(|z - z'|)}{\partial z^2} = \frac{1}{\lambda^2}h(|z - z'|), \tag{9}$$

where $h(|z|)$ is the force correlation function [22]. It is worth noting that, when applying (9) to the former potentials (6)–(8), the underlying forces exhibit negative spatial correlations [22], as well as a positive part.

The forces used in the Langevin equation at the lattice points of one potential are obtained by simple centered discrete derivatives. The random force at intermediate locations is evaluated by standard linear interpolation of the forces at the lattice points. Explicit details are given in Ref. [22].

Transport and diffusion anomalies are explored through statistical averages, specifically through first moments and second cumulants of the trajectories $z(\tau)$. In particular, transport is analyzed through the first moment

$$\langle z(\tau)\rangle \propto \tau^{\alpha}. \tag{10}$$

When $\alpha = 1$ there is normal transport and the mean velocity $\langle v\rangle = \langle z(\tau)\rangle/\tau$ is constant. In contrast, $\alpha \neq 1$ leads to anomalous transport, either subtransport $\alpha < 1$ or supertransport $\alpha > 1$.

The time dependence of the variance or second cumulant is usually written as

$$\langle\Delta z^2(\tau)\rangle \propto \tau^{\beta}. \tag{11}$$

Three different regimes are also possible here: subdiffusive ($\beta < 1$), superdiffusive ($\beta > 1$), and diffusive ($\beta = 1$). In this last regime we recover the familiar form $\langle\Delta z^2(\tau)\rangle = 2D\tau$, where D is the diffusion coefficient. The exponents α and β can be obtained by fitting a power-law function of time to the statistical moments $\langle z(\tau)\rangle$ and $\langle\Delta z^2(\tau)\rangle$; β can be also evaluated from the expression

$$\beta = \log_{10}\left[\frac{\Delta z^2(10\tau)}{\Delta z^2(\tau)}\right], \tag{12}$$

which gives a series of β values that might converge to a limit.

III. SIMULATION RESULTS AND ANOMALOUS EXPONENTS IN ONE DIMENSION

The Langevin equations are numerically integrated following a second-order Heun algorithm for ordinary stochastic differential equations [23] and the random potential is generated following the explicit procedures described in Ref. [22]. One hundred particles are used in each realization of 100 disordered potentials, so the statistical averages are over 10 000 particles. We expect this to be sufficient to get reliable information about the transport and diffusion properties of the system. Particles are initially distributed uniformly along a large region of the potential landscape of size $20\,000\lambda$. Therefore, each particle of the 100 in a given potential is likely to experience a different and independent portion of the potential. The potential landscape covers $N = 2^{23}$ lattice points with periodic boundary conditions and a lattice constant $\Delta = 0.1$. Other parameter values are $\mathcal{T} = 0.1$ and disorder correlation length $\lambda = 1$. To explore the different anomalous regimes we have used the force $\mathcal{F}$ as a control parameter.

The time integration step $\Delta\tau$ should be chosen so that in each integration step particles do not move over a distance greater than that associated with the roughness of the potential. That is, $\Delta\tau \ll \lambda_{\rm rgh}/\mathcal{F}$, where $\lambda_{\rm rgh}$ is the length scale of the roughness of the disorder. We also require the asymptotic mean velocity for particles under large external forces to obey the relation $\langle v\rangle \propto \mathcal{F}$. Using these conditions, we have settled on the value $\Delta\tau = 0.1$ for the Gaussian and the power-law correlated potentials. On the other hand, $\Delta\tau = 0.01$ is required

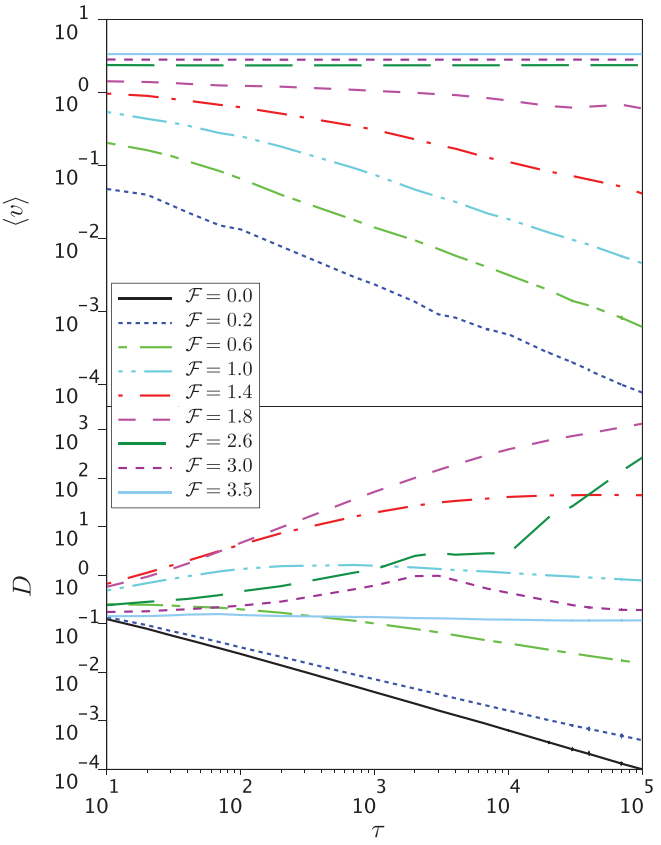

FIG. 1. (Color online) Temporal evolutions of the velocity (top) and diffusion (bottom). Simulation of the Langevin equation were performed for 100 particles and 100 realizations of the potential with Gaussian correlation.

for the potential with a double-sided exponential correlation because of the smaller roughness length scale associated with the singularity exhibited by its first derivative at the origin.

In addition to this set of reference parameters, we have also explored other values: $\mathcal{T} = 0.05$, $\Delta = 0.05$ (with $N = 2^{24}$), and $\Delta\tau = 0.005$ and 0.001. No qualitative changes have been noted in the outcome, yet remarkable quantitative differences emerge, especially when changing Δ and $\Delta\tau$ for the double-sided exponential correlation. We discuss this further in detail below.

Different time evolutions of the mean velocity and diffusion coefficient for the case of Gaussian disorder are shown in a log-log plot in Fig. 1 for different values of the external force. Time-independent lines, that is, normal behavior, are hardly observed in these figures. Furthermore, in some domains of the force, straight lines are clearly seen, which is convincing evidence of the existence of exponents different from those of normal transport and diffusion. Specifically, it can be gathered that weak forces induce subtransport, while normal behavior is recovered for stronger ones. Moreover, intermediate anomalous regimes are also seen for diffusion: subdiffusion for weak forces, superdiffusion for intermediate forces, and normal diffusion for very strong forces. We note the occurrence of a fourth special regime before the recovery of diffusion following superdiffusion. In this regime, diffusion cannot be specified from the numerical results, but transport is

TABLE I. Exponents α (bottom left) and β (upper right) of the first moment (10) and the variance (11) of the trajectories given by the simulation of Eq. (4). Different disorder types are Gaussian correlated (6) (Gaussian), double-sided exponential correlated (7) (Exponential), and power-law correlated (8) with $\varepsilon = 1/3$ (Pl 1/3) and $\varepsilon = 2/3$ (Pl 2/3). A minus sign means that there is no transport. A plus sign labels those cases in which the variance trajectories have uncertain time behavior. An n means that simulations have been avoided since it is quite clear that the normal regime is expected.

α \ β	Gaussian	Exponential	Pl 1/3	Pl 2/3
$\mathcal{F}$ =0.0	0.20 / –	0.24 / –	0.33 / –	0.33 / –
0.2	0.36 / 0.29	0.36 / 0.27	0.88 / 0.47	0.60 / 0.36
0.4	0.48 / 0.28	0.53 / 0.34	1.29 / 0.64	0.84 / 0.42
0.6	0.58 / 0.32	0.63 / 0.34	1.56 / 0.89	1.11 / 0.54
0.8	0.67 / 0.33	0.74 / 0.32	1.45 / 1.00	1.32 / 0.64
1.0	0.84 / 0.40	0.84 / 0.46	+ / 1.00	1.54 / 0.91
1.2	0.96 / 0.41	0.93 / 0.53	+ / 1.00	1.51 / 1.00
1.4	1.07 / 0.58	1.03 / 0.46	0.94 / 1.00	1.72 / 1.00
1.6	1.23 / 0.64	1.12 / 0.54	0.98 / 1.00	+ / 1.00
1.8	1.51 / 0.90	1.21 / 0.66	0.99 / 1.00	+ / 1.00
2.0	1.60 / 0.99	1.31 / 0.72	0.99 / 1.00	+ / 1.00
2.5	+ / 1.00	1.40 / 0.84	n	0.99 / 1.00
3.0	+ / 1.00	1.58 / 0.96	n	1.00 / 1.00
3.5	0.98 / 1.00	1.44 / 0.99	n	n
4.0	0.99 / 1.00	+ / 1.01	n	n
4.5	n	+ / 1.00	n	n
5.0	n	+ / 1.00	n	n
5.5	n	+ / 1.00	n	n
6.0	n	1.00 / 1.00	n	n

normal and thus it might be referred to as an uncertain regime. We will continue this discussion later on.

The effects of the different disorder correlations on the transport and diffusion regimes as functions of the external force are checked via the resulting α and β exponents, both displayed in Table I and depicted in Fig. 2. In the figure we can see that the same transport and diffusion regimes are reached despite the differences in the random potential correlations, that is, roughly speaking, subtransport ($\alpha < 1$) and subdiffusion ($\beta < 1$) at weak forces and normal behavior at high forces ($\alpha = 1$, $\beta = 1$). Meanwhile, for intermediate

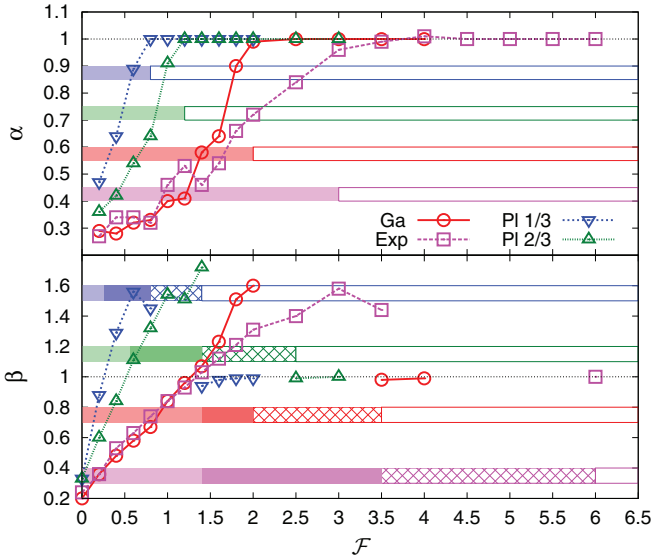

FIG. 2. (Color online) Transport (top) and diffusion (bottom) exponents for different distributions of disorder. The parameters are the same as in Fig. 1, with $\varepsilon = 1/3$ and $2/3$ for the power-law case. Wide horizontal colored bars (shown from bottom to top are Exp, Ga, Pl 1/3, and Pl 2/3 disorder) indicate each dynamical regime (as described in the text).

forces, diffusion exhibits two different regimes: superdiffusion ($\beta > 1$) and uncertain diffusion. Figure 2 also shows the force interval associated with every dynamical regime (transport in the upper graphic, diffusion in the lower) for each of the four types of potential correlations (color coded bars). Indeed, subtransport (weakly colored filled bar) and normal transport (empty bar) appear on the plots of the α values for all the potentials (top). Subdiffusion (weakly colored filled bar), superdiffusion (colored filled bar), uncertain diffusion (patterned bar), and diffusion (empty bar) are evident in the β values for all the potentials (bottom). This figure allows us to conclude that the length of each dynamical regime is controlled by the correlation of the disorder. In particular, using an effective correlation length λ_{eff} defined as $g(\lambda_{\text{eff}}/\lambda) = 0.25$ (Fig. 3) allows us to conclude that a larger λ_{eff} leads to an earlier (in terms of force) recovery of the normal transport and diffusion regimes.

Figure 3 (bottom) displays the landscapes of the potentials with the same realization of random numbers, from which it can be noted that larger λ_{eff} are linked with landscapes with shallower wells. It follows that the smoother a potential is, the weaker the forces that are needed to achieve normal transport and diffusion for Brownian motion in these potentials. This inference is in agreement with the interpretation of anomalous Brownian motion as a consequence of the interplay of locked and running states [12]. Roughly speaking, in a smoother potential tilted by a force, thermal fluctuations are more likely to help the particles overcome its barriers and thus normal behavior is recovered more easily.

Power-law correlated potentials are characterized not only by the length scale but also by the tail exponent ε and thus they require a separate discussion. From Fig. 3 it can be seen that, roughly speaking, λ_{eff} is inversely proportional to ε. Therefore

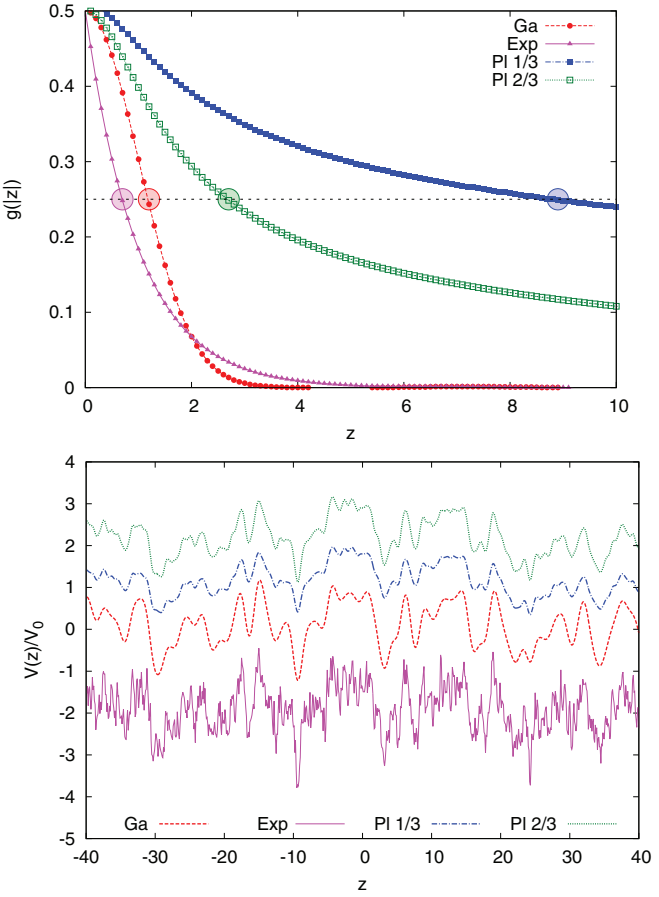

FIG. 3. (Color online) The top shows correlation functions $g(|z|)$ for the Gaussian (Ga), double-sided exponential with discretization $\Delta = 0.1$ (Exp), and power law with $\varepsilon = 1/3$ (Pl 1/3) and $\varepsilon = 2/3$ (Pl 2/3). Colored circles at $g(|z|) = 0.25$ provide a measure of the effective correlation lengths. The bottom shows potential landscapes for each case; $\lambda = 1$ for all cases. A vertical shift is implemented for better visualization (2, 1, and -2 potential units for Pl 2/3, Pl 1/3, and Exp, respectively).

the arguments involving ε might be expected to be opposite to those invoked for λ_{eff}. However, the λ_{eff} argument fails to explain the outcomes of the simulations for double-sided exponentially correlated disorder, which might be expected to be closer to those of the Gaussian disorder since they have similar values of λ_{eff}. The reason is that the exponentially correlated potential exhibits a second much finer structure of tiny wells due to the shorter spatial scale related to the discretization length Δ. This secondary structure is hardly affected by the action of the external force because of the large characteristic slope of the potential. Indeed, once the primary structure has almost been counterbalanced by $\mathcal{F}$, these secondary tiny wells associated with the Δ length scale still remain. That is the reason why both the superdiffusive and the uncertain diffusive regimes for these disorders prevail up to higher forces compared to the Gaussian disorder. We may thus assert that for the double-sided exponentially correlated potential, the λ_{eff} length scale controls the subdiffusive regime, whereas superdiffusion and uncertain diffusion are controlled by the Δ length scale.

Transport regimes associated with the Gaussian and double-sided exponential correlated disorders show the same trend up to a certain force, after which the trends diverge and the normal transport recovery is delayed for the exponential case. The force at which the two behaviors begin to diverge turns out to be precisely the force at which both systems become superdiffusive and thus the former argumentation is reinforced. As to the transport behavior, the secondary scale Δ leads to a decrease of the velocity of the particles because of the presence of small obstacles and thus subtransport prevails longer.

These results lead us to further consider the case of double-sided exponentially correlated disorder, now with a smaller discretization parameter than considered above, namely, $\Delta = 0.05$. Compared to the case with $\Delta = 0.1$, the smaller discretization parameter is associated with a higher degree of roughness in the secondary scale. Our earlier arguments then lead us to conclude that the time step $\Delta\tau = 0.01$ might not be sufficiently small to accurately capture the behavior of the system. We pick the smaller time step $\Delta\tau = 0.001$. While the behavior of transport and diffusion are essentially the same as in the case of the exponential correlation with $\Delta = 0.1$, the superdiffusive and uncertain diffusive regimes are extended in the case of $\Delta = 0.05$. This reinforces the idea that the secondary roughness associated with the Δ length scale regulates the persistence of superdiffusion and uncertain diffusion.

We note a qualitative similarity between behaviors observed here and in the case of underdamped Brownian particles in a periodic potential [24]. In both cases there is a regime of forces where some particles are in a running state of essentially deterministic velocity $v \sim \mathcal{F}$ while others are in a locked or trapped state of zero velocity. In our random potentials there is thus a large variation of the particle distribution and of the motion of the particles for different realizations of the potentials, leading to anomalous dispersion, and thus to the uncertain diffusive regime, much as is observed in the underdamped problem.

Finally, the asymptotic temporal behavior of transport and diffusion deserves a separate comment. The time variable τ can be compared to a characteristic time of the system to provide a sense of the temporal extent of our simulations. One can define the deterministic time τ_0 that it takes to cover a distance λ under the action of a force $\mathcal{F}$,

$$\tau_0 = \frac{\lambda}{\mathcal{F}}, \tag{13}$$

which in our systems lies in the domain $\tau_0 \in (0.33, 2.0)$. Our simulations run as far as five decades of this characteristic time. Several anomalies are observed over this full interval while others are shorter, with a duration two or three decades of this time. Recently this problem was addressed in Ref. [13], with similar qualitative results: the presence of a subdiffusive regime. However, we cannot assert that even with longer simulation times normal transport and diffusion will be achieved. While it is commonly accepted that at asymptotic times all behaviors will be normal and diffusive, from the experimental point of view time is finite and it would be helpful to know if important anomalies appear in realistic observation time intervals. These interpretations of our results are appropriate provided the total simulation time is large enough without running into finite-system-size effects. The total length of our system is $\approx 8.39 \times 10^5$, but the system is periodic, so we should avoid covering more than half of this distance, $\approx 4.2 \times 10^5$. For a force of $\mathcal{F} = 3.5$ and a maximum time of $\tau = 10^5$, particles travel as far $\approx 3.34 \times 10^5$, that is, at most of the same order as half the length. For times much larger than this one can expect finite-size effects and, accordingly, normal behavior.

IV. EVOLUTION OF PARTICLE DENSITY

We next explore the behavior of the particle density representative of the various combinations of behaviors discussed above. In Fig. 4 we present the histogram of the relative displacements $z(\tau) - \langle z(\tau) \rangle$ of all the particles for various values of the external force and under a Gaussian disordered potential, where the angular brackets indicate an average over all the particles. From top to bottom, $\mathcal{F} = 0.6$, 1.8, 2.6, and 4.0. These cases are chosen as representative of the variety of anomalies: subtransport and subdiffusion [Fig. 4(a)], subtransport and superdiffusion [Fig. 4(b)], the uncertain diffusive regime [Fig. 4(c)], and the case of both normal transport and diffusion [Fig. 4(d)].

A system with weak forces ($\mathcal{F} = 0.6$) presents subtransport and subdiffusion [see Fig. 4(a)], with an asymmetric

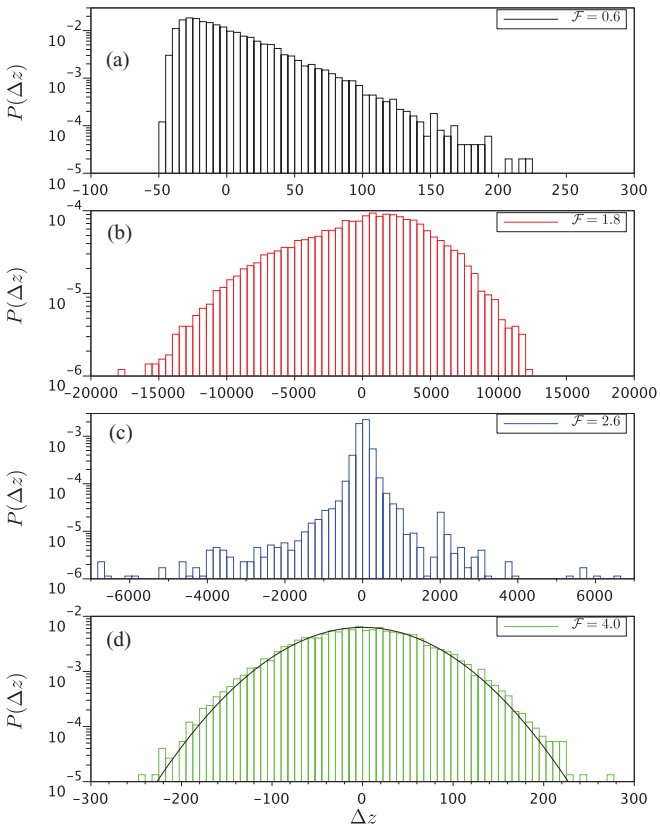

FIG. 4. (Color online) Displacement distribution of the particles $P(\Delta z)$ for different combinations of displacements and diffusions. $\mathcal{F} = 0.6$ (a), 1.8 (b), 2.6 (c), and 4.0 (d) at $\tau = 20\,000$. It is important to pay attention to the horizontal scale in each plot. Plot (d) includes the representation of a Gaussian function of zero mean ($\mu = 0$) and variance $\sigma^2 = 2D\tau$ ($D = \mathcal{T} = 0.1$, $\tau = 20\,000$).

displacement distribution with a long forward exponential tail and as a consequence with its maximum shifted towards negative displacements. A few particles pull ahead, but most are stuck. This behavior is enhanced as time proceeds.

When the force increases up to $\mathcal{F} = 1.8$, there is sub-transport as well, but with superdiffusion. In this case, the displacement distribution [Fig. 4(b)] is also asymmetric, but now with a backward larger tail and the maximum shifted to the right. Many particles are still stuck, but a larger number of them now pull ahead. Note that the dispersion is much larger than in the previous case.

For a stronger force $\mathcal{F} = 2.6$, the transport is normal $\langle v \rangle \sim \mathcal{F}$, but our simulation data are not sufficient to obtain a reliable result to characterize the diffusion. The distribution in Fig. 4(c) also lacks symmetry. It shows a very narrow maximum, which is the signature of the running state of most of the particles, even while there may still be a few particles in the locked state $\langle v \rangle \sim 0$, which may become trapped in the few realizations of the potential that present the deepest wells. (Figure 9 in the following section is helpful for a better understanding.)

The figure with the highest force $\mathcal{F} = 4.0$ [Fig. 4(d)] illustrates normal behavior, i.e., normal transport and normal diffusion, with a Gaussian-like distribution, as confirmed by the solid Gaussian curve ($\mu = 0$, $\sigma^2 = 2D\tau$, $D = \mathcal{T} = 0.1$, $\tau = 20\,000$). Essentially perfect Gaussian behavior is expected for very large forces.

V. TRANSPORT AND DIFFUSION OF PARTICLES ON SURFACES

The 2D overdamped Langevin equation is a straightforward generalization of Eq. (4) for the x and y coordinates of the particle. Transport and diffusion in two dimensions exhibit different phenomena because one can study the orthogonal direction with respect to the force. In Cartesian coordinates the force is written as

$$\vec{\mathcal{F}} = \mathcal{F}\hat{u}_\parallel = \mathcal{F}(\cos\theta\,\vec{i} + \sin\theta\,\vec{j}), \tag{14}$$

which defines the parallel unit vector $\hat{u}_\parallel$. The perpendicular unit vector is $\hat{u}_\perp = -\sin\theta\,\vec{i} + \cos\theta\,\vec{j}$. The simulated trajectories yield the Cartesian components of the average velocity $\langle\vec{v}\rangle = (\langle v_i\rangle, \langle v_j\rangle)$ and the Cartesian diffusion tensor $\mathcal{D} = \{D_{ij}\}$. With this information, transport and diffusion in any direction $\hat{u}$ can be computed

$$\langle v_u \rangle = \langle\vec{v}\rangle \cdot \hat{u}, \quad D_u = \hat{u} \cdot \mathcal{D} \cdot \hat{u}. \tag{15}$$

TABLE II. Transport $\alpha_\parallel$ and diffusion $\beta_\parallel$ and $\beta_\perp$ exponents obtained by a power-law regression of the curves in Fig. 5 and the application of Eq. (12) to Fig. 6. The plus sign denotes a case where the diffusion coefficient cannot be extracted from the simulation data.

$\mathcal{F}$	$\alpha_\parallel$	$\beta_\parallel$	$\beta_\perp$
0.6	0.11	0.43	0.20
1.0	0.18	0.59	0.38
1.2	0.32	1.00	0.42
1.3	0.57	1.36	0.47
1.5	0.80	2.01	0.82
2.0	1.00	+	0.99
3.0	1.00	1.01	1.02

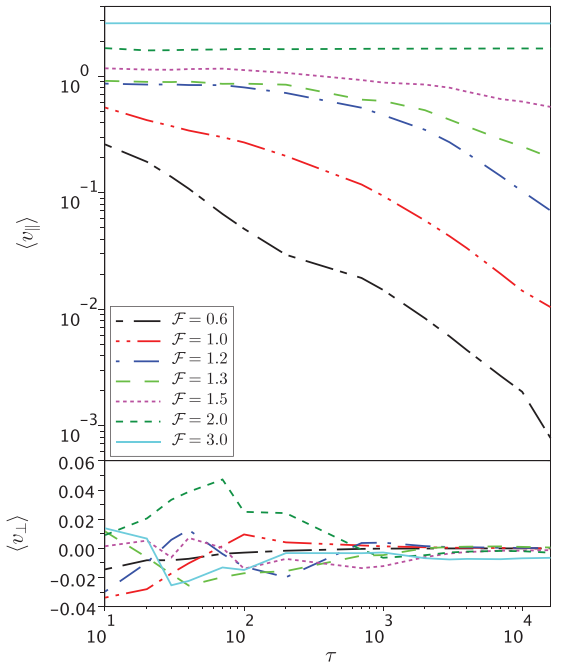

FIG. 5. (Color online) Parallel (top) and perpendicular (bottom) mean velocities of 400 particles, averaged over 20 realizations of the random potential surface, with $\theta = \arctan(100/N\Delta)$.

The choices of the angles at which to perform the simulations can be made so as to provide the maximum amount of information, as follows. If $\theta = 0$, we would see that the cloud of particles might reach the system size quite fast without exploring the whole landscape. Periodic boundary

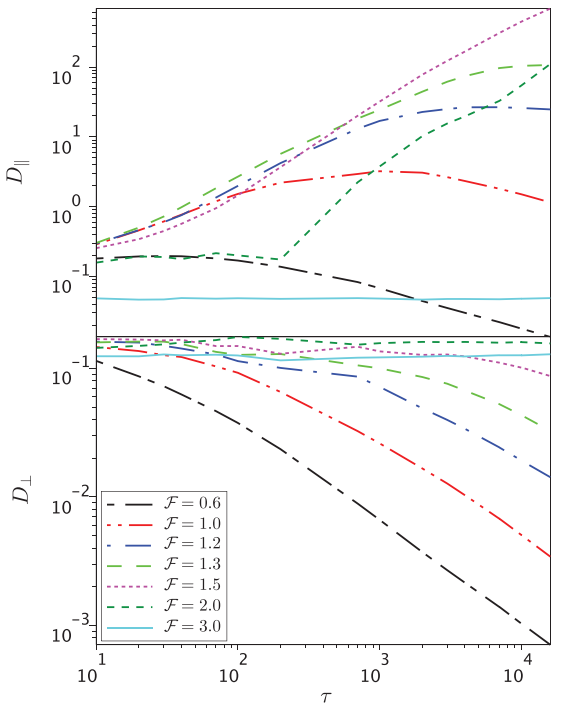

FIG. 6. (Color online) Parallel (top) and perpendicular (bottom) diffusion coefficients. The parameters are the same as in Fig. 5.

conditions are not helpful in this case. This is clearly not a particularly informative choice. In contrast, a finite θ along with periodic boundary conditions produces a spiraling motion along a torus. Therefore, helpful choices of θ are the ones that prevent intersection (or statistical correlation) between particle trajectories that coil the torus after each turn while allocating the maximum number of loops. We have made such choices.

We have studied overdamped Brownian particles moving in 2D Gaussian correlated disorder

$$g(|\vec{r}-\vec{r}'|) = \tfrac{1}{2} e^{-[(\vec{r}-\vec{r}')\cdot(\vec{r}-\vec{r}')/2\lambda^2]}. \tag{16}$$

This correlation is isotropic and does not introduce a bias in any direction. The simulations were run on a lattice of $N^2 = 4096^2$ sites with $\Delta x = \Delta y = 0.5$. The other simulation parameters were $\Delta\tau = 0.1$ and $\mathcal{T} = 0.03$. The temperature is much lower than in the 1D simulations because particles might avoid the highest potential barriers by changing their direction.

As in the one-dimensional problem, we compute the first moment and the second cumulant on the ensemble of trajectories, now separately for the directions parallel and perpendicular to $\vec{\mathcal{F}}$. This allows the fitting of the transport $(\alpha_\parallel,\alpha_\perp)$ and diffusion $(\beta_\parallel,\beta\perp)$ exponents. These results are included in Table II. The corresponding time dependence of the velocity $(\langle v\rangle_\parallel,\langle v\rangle_\perp)$ and the diffusion coefficients $(D_\parallel,D_\parallel)$ are shown in Figs. 5 and 6, respectively.

Along the orthogonal direction (Fig. 5, bottom) we find no transport ($\langle v_\perp\rangle \approx 0$), yet there is subdiffusive dispersion (Fig. 6, bottom), as should be expected since no force is present [8]. The phenomenology in the parallel direction is the same as in the 1D case. Now we have a different interesting situation: For intermediate forces the dispersion displays parallel superdiffusion with perpendicular subdiffusion.

We also plot the cloud of particle positions at different times for some representative behaviors along the direction parallel to the external force: subdiffusion with subtransport ($\mathcal{F} = 0.6$) in Fig. 7, superdiffusion and subtransport ($\mathcal{F} = 1.5$) in Fig. 8, no well defined diffusion in Fig. 9 ($\mathcal{F} = 2.0$), and both normal diffusion and transport ($\mathcal{F} = 3.0$) in Fig. 10. The differences in the horizontal scales of the four figures should be noted. The clouds are plotted on the same scales for the x and y directions to highlight the respective asymmetries.

For small forces, the majority of the particles are expected to be trapped most of the time. A few of them might undergo short random displacements with a bias toward the direction of the force. That is seen in Fig. 7 (top) for $\mathcal{F} = 0.6$, in which the cloud spreads in the parallel direction showing some kind

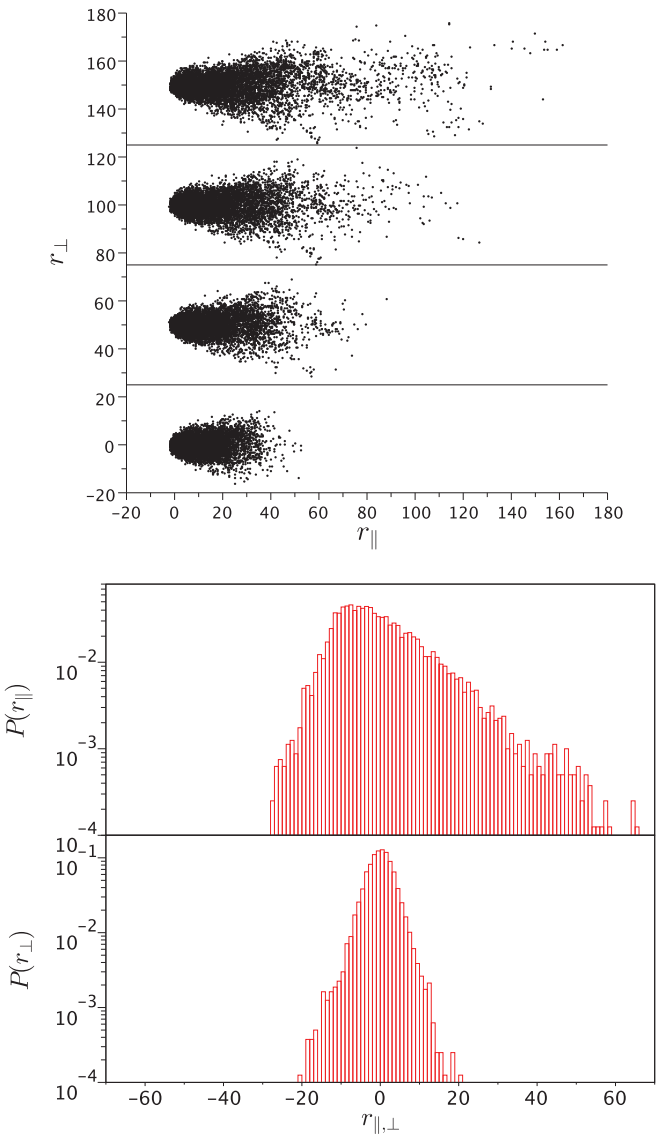

FIG. 7. (Color online) The top shows particle positions with respect to initial conditions at different times for $\mathcal{F} = 0.6$ and, from bottom to top, $\tau = 250, 1000, 4000, 16\,000$. The bottom shows the particle displacement distribution at $\tau = 1000$ along the parallel (top) and perpendicular (bottom) directions relative to the force.

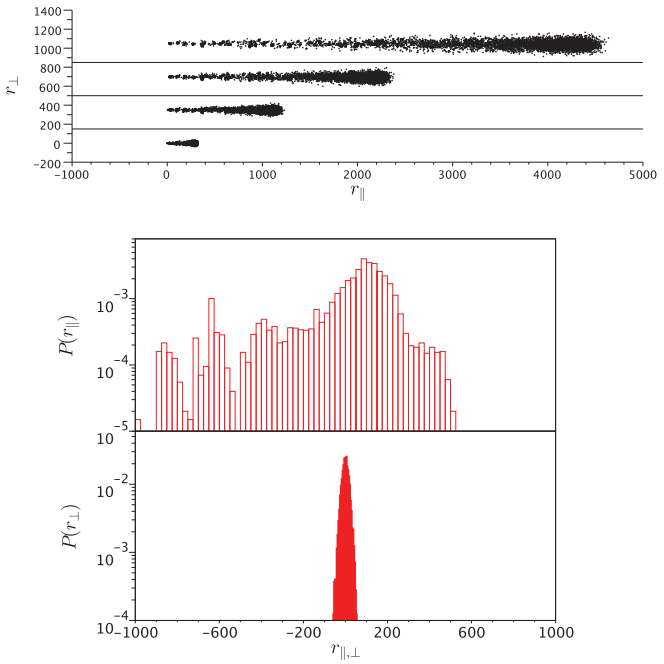

FIG. 8. (Color online) The top shows particle positions relative to the initial condition at different times for $\mathcal{F} = 1.5$ and, from bottom to top, $\tau = 250, 1000, 2000, 4000$. The bottom shows the particle displacement distribution at $\tau = 1000$ along the parallel (top) and perpendicular (bottom) directions relative to the direction of the force.

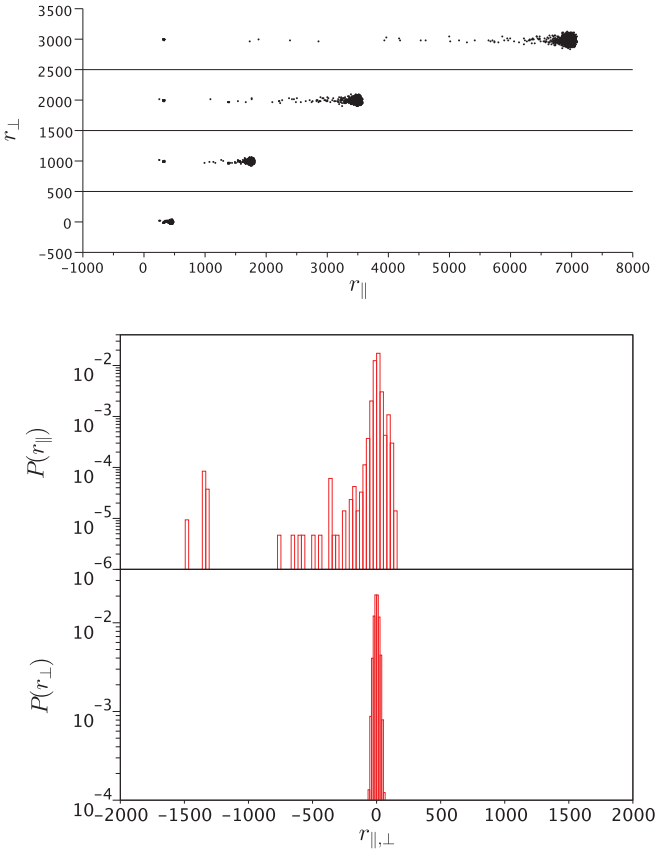

FIG. 9. (Color online) The top shows particle positions relative to the initial conditions at different times for $\mathcal{F} = 2.0$ and, from bottom to top, $\tau = 250, 1000, 2000, 4000$. The bottom shows the particle displacement distribution at $\tau = 1000$ along the parallel (top) and perpendicular (bottom) directions relative to the direction of the force.

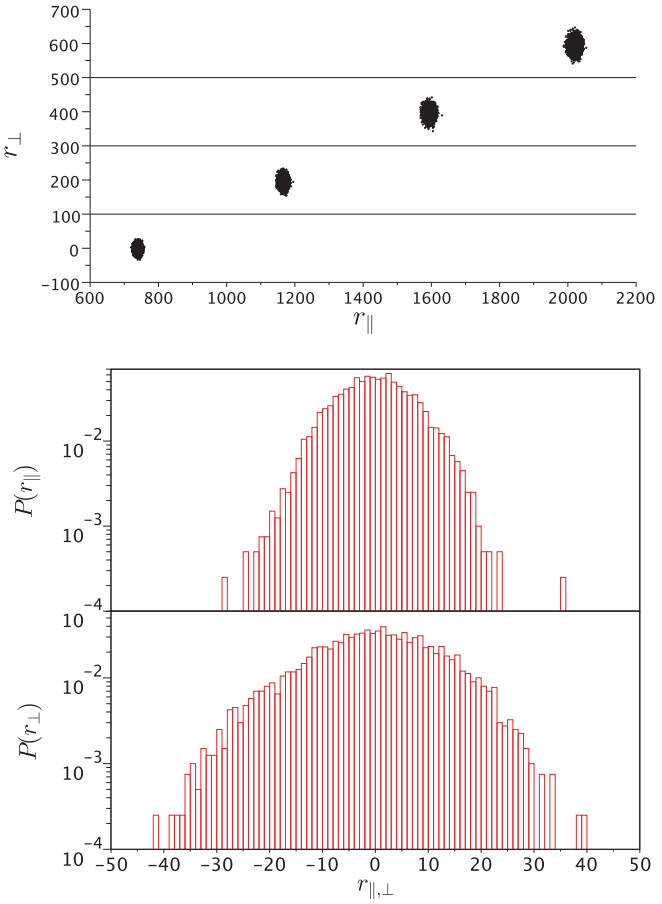

FIG. 10. (Color online) The top shows the particle cloud at different times for $\mathcal{F} = 3.0$ and, from bottom to top, $\tau = 250, 400, 550, 700$. The bottom shows the particle displacement distribution at $\tau = 1000$ along the parallel (top) and perpendicular (bottom) directions relative to the direction of the force.

of a forward comet tail. Besides, particles in this tail are more likely to spread along the perpendicular direction as well since they are the ones that have avoided the deepest wells along their trajectories. This information is complemented by the histograms of the particle positions in both directions (Fig. 7, bottom) where the asymmetry in the parallel direction contrasts with the symmetry in the perpendicular one.

In the superdiffusive regime, along the parallel direction ($\mathcal{F} = 1.5$) we see a cometlike figure with a larger density at its head. Thus, while no big differences in the dispersion are seen in the perpendicular direction between $\mathcal{F} = 1.5$ and 0.6, there is a very large increase of the dispersion in the parallel direction and, in addition, its asymmetry is in the opposite direction, i.e., it has a backward long tail. The corresponding histograms in Fig. 8 (bottom) corroborate the top panel.

The intermediate value of the force $\mathcal{F} = 2.0$ corresponds to the regime in which it is not possible to define an anomalous exponent for the diffusion. The cloud evolution under this condition (Fig. 9, top) exhibits a front of particles that travels at a deterministic velocity of about $v_{\text{cloud}} \approx \mathcal{F}$, while others are trapped in a few positions towards the back that may belong to few realizations of the disordered surface. This picture, together with the parallel histogram in Fig. 9 (bottom), reinforces the argumentation developed earlier for $\mathcal{F} = 2.6$ in the case of unidimensional Gaussian correlated disorder.

Finally, for a large force $\mathcal{F} = 3.0$, normal transport and diffusion in both directions are recovered. These phenomena are featured in Fig. 10 (top), in which elliptical clouds travel along the parallel direction with a velocity $v_{\text{cloud}} \approx 3 \approx \mathcal{F}$. Although there is normal diffusion along both directions, the elliptical shape reveals a different diffusion coefficient for each direction. This result is clearly confirmed by the corresponding histogram (Fig. 10, bottom), in which we observe a wider Gaussian distribution in the direction perpendicular to the external force. This is not unexpected since the external force breaks the symmetry of the system, that is, it smoothes the potential barriers along its direction.

VI. CONCLUSION

Transport and diffusion of unidimensional overdamped Brownian particles in totally disordered potentials show anomalous regimes whose strength and external force dependence in turn depend on the temperature $\mathcal{T}$ and the statistical properties of the disorder. This dependence can be understood via the theoretical consideration of anomalous Brownian motion already developed in Ref. [12]. In addition,

the length scales of the roughness of the potentials have been shown to be essential parameters in the understanding of the effect of disorder in anomalous regimes.

The main practical difference between different kinds of disorder can be associated with an effective correlation length. Taking the Gaussian correlation as a reference, we see that power-law correlations present a larger effective length and, accordingly, shallower wells, which implies that normal regimes appear sooner. On the other hand, double-sided exponential correlations, despite having a similar effective length scale, also exhibit a second much smaller length scale associated with the space discretization length Δ. This length scale causes the appearance of a secondary structure composed of tiny wells, yet with higher roughness (steep landscape slopes). Its importance becomes evident when the force is sufficiently strong to overcome the primary structure (associated with λ_{eff}). It requires higher forces for the recovery of normal transport since it obstructs the free displacement of the particles even when the primary structure of obstacles has already been overcome. Both superdiffusion and uncertain diffusion thus continue to occur up to higher forces because of the continued simultaneous presence of running states and locked states, the latter now due to the small wells associated with Δ. More generally, we conclude that when disorder exhibits two different length scales, subdiffusion is associated with the longer one and both superdiffusion and uncertain diffusion are associated with the shorter one.

The evolution of the particle density in Fig. 4 and 7–10 reveals other interesting characteristics of the anomalies. Each different asymmetry of the histogram is related to subdiffusion and superdiffusion regimes for finite forces. The non-Gaussian-like form of these distributions is thus an indicator that some anomaly is present.

For two dimensions, a completely different behavior of transport and diffusion is seen between the directions perpendicular and parallel to the force. We especially note the coexistence of subdiffusion and superdiffusion along different spatial directions.

The uncertain diffusive regime is caused by the finite number of particles and of realizations of disordered potentials. A small number of locked particles have a great effect, leading to uncertain behavior of the statistical moments of the position of the particles.

Finally, concerning either 1D or 2D results, it should be noted that transport and diffusion anomalies have not been proved to be steady-state regimes. However, simulation data show that anomalies span several decades of time.

ACKNOWLEDGMENTS

This work was supported by the Spanish DGICYT Project No. FIS2012-37655-C2-2 and the Generalitat de Catalunya Project No. 2009SGR14. K.L. gratefully acknowledges the support of the NSF under Grant No. PHY-0855471.

[1] P.-G. de Gennes, J. Stat. Phys. **12**, 463 (1975).
[2] H. Bassler, Phys. Rev. Lett. **58**, 767 (1987).
[3] R. Zwanzig, Proc. Natl. Acad. Sci. USA **85**, 2029 (1988).
[4] D. H. Dunlap, P. E. Parris, and V. M. Kenkre, Phys. Rev. Lett. **77**, 542 (1996).
[5] P. E. Parris, M. Kuś, D. H. Dunlap, and V. M. Kenkre, Phys. Rev. E **56**, 5295 (1997).
[6] J. P. Bouchoud and A. Georges, Phys. Rep. **195**, 127 (1990).
[7] J. M. Sancho and A. M. Lacasta, Eur. Phys. J. Spec. Top. **187**, 49 (2010).
[8] A. H. Romero and J. M. Sancho, Phys. Rev. E **58**, 2833 (1998).
[9] K. Lindenberg, J. M. Sancho, M. Khoury, and A. M. Lacasta, Fluct. Noise Lett. **11**, 1240004 (2012).
[10] P. Reimann and R. Eichhorn, Phys. Rev. Lett. **101**, 180601 (2008).
[11] M. Khoury, J. P. Gleeson, J. M. Sancho, A. M. Lacasta, and K. Lindenberg, Phys. Rev. E **80**, 021123 (2009).
[12] M. Khoury, A. M. Lacasta, J. M. Sancho, and K. Lindenberg, Phys. Rev. Lett. **106**, 090602 (2011).
[13] R. D. L. Hanes and S. U. Egelhaaf, J. Phys. Condens.: Matter **24**, 464116 (2012); F. Evers, C. Zunke, R. D. L. Hanes, J. Bewerunge, I. Ladadwa, A. Heuer, and S. U. Egelhaaf, Phys. Rev. E **88**, 022125 (2013).
[14] S.-H. Lee and D. G. Grier, Phys. Rev. Lett. **96**, 190601 (2006).
[15] R. D. L. Hanes, M. Schmiedeberg, and S. U. Egelhaaf, arXiv:1309.4801v1.
[16] M. Slutsky, M. Kardar, and L. A. Mirny, Phys. Rev. E **69**, 061903 (2004).
[17] M. Weiss, Phys. Rev. E **88**, 010101 (2013).
[18] M. Schunack, T. R. Linderoth, F. Rosei, E. Laegsgaard, I. Stensgaard, and F. Besenbacher, Phys. Rev. Lett. **88**, 156102 (2002).
[19] Q. Xu, L. Feng, R. Sha, N. C. Seeman, and P. M. Chaikin, Phys. Rev. Lett. **106**, 228102 (2011).
[20] A. S. de Wijn, Phys. Rev. E **84**, 011610 (2011).
[21] M. J. Skaug, J. Mabry, and D. K. Schwartz, Phys. Rev. Lett. **110**, 256101 (2013).
[22] M. Suñé, J. M. Sancho, and A. M. Lacasta, Fluct. Noise Lett. **11**, 1250026 (2012).
[23] J. Garcia-Ojalvo and J. M. Sancho, *Noise in Spatially Extended Systems* (Springer, New York, 1999).
[24] K. Lindenberg, J. M. Sancho, A. M. Lacasta, and I. M. Sokolov, Phys. Rev. Lett. **98**, 020602 (2007).